POLITECNICO DI TORINO
Repository ISTITUZIONALE

CFD Analysis of a Simple Orifice-Type Feeding System for Aerostatic Bearings

Original
CFD Analysis of a Simple Orifice-Type Feeding System for Aerostatic Bearings / Belforte, G., Raparelli, T., Trivella, A., Viktorov, V., Visconte, C.. - In: TRIBOLOGY LETTERS. - ISSN 1023-8883. - STAMPA. - 58:25(2015). [10.1007/s11249-015-0503-8]

Availability:
This version is available at: 11583/2597359 since: 2017-01-24T14:17:26Z

Publisher:
Springer

Published
DOI:10.1007/s11249-015-0503-8

Terms of use:

This article is made available under terms and conditions as specified in the corresponding bibliographic description in the repository

Publisher copyright

(Article begins on next page)

27 November 2026

CFD analysis of aerostatic pads with simple orifice-type feeding system

G. Belforte, T. Raparelli, A. Trivella, V. Viktorov, C. Visconte

Politecnico di Torino, Department of Mechanical and Aerospace Engineering

Corso Duca degli Abruzzi, 24

10129 TORINO, Italy

Tel: +39 011 090 6925, Fax: +39 011 090 6999, e-mail: carmen.visconte@polito.it

Authors' version (final draft post-refereeing)

Published in:

***Tribology Letters*, 58(2) (2015), Article 25**

DOI: 10.1007/s11249-015-0503-8

ABSTRACT

A numerical analysis on the feeding system of externally pressurized gas bearings, for the correction of the theoretical mass flow rate formula by means of a discharge coefficient, is presented. A flat aerostatic pad with a simple orifice-type feeding system was chosen as case on study, the authors having previously carried out experimental tests on such a prototype. Using the commercial CFD code Ansys Fluent ®, preliminary simulations were carried out on a pad's geometry using three different flow models. Having selected the flow model able to give the best prediction of the pad's behaviour in terms of pressure distribution along the air film, additional simulations were carried out on pads with two different diameters of the supply hole, varying the film thickness in a range from 9 to 14 μm.. A comparison between numerical and experimental results is presented. In addition, the effect of the flow intake used to perform experimental tests and of the shape of the orifice's external edge on pressure distribution is analysed.

Keywords: aerostatic pads, discharge coefficient, numerical simulation

1. INTRODUCTION

Air bearings are widely employed for their low friction loss in applications where high precision positioning and, more recently, high rotary speed are demanded. Air, continuously flowing from an

external source to atmosphere between the two faced bearing surfaces, acts as lubricant and, at the same time, gives the bearing the capability to support an external load.

The flow characteristics of air bearings are strongly dependent on the geometry of the supply system and on the air film thickness. Usually, simple orifice-type or pocketed orifice-type restrictors are used as supply systems [1]; in both cases, measuring the supply holes' downstream pressure and the pressure distribution along the air film is fundamental for predicting air pads behaviour [2] [3]. Different methods have been proposed to calculate mass flow-rate in these devices, as discussed in [4]. A common approach consists in treating the supply system as a local resistance; as a consequence, the mass flow rate G can be calculated as:

$$G = C_d \cdot G_t \qquad (1)$$

where G_t is the theoretical mass flow rate (isentropic expansion), worked out as for an ideal nozzle, and C_d is a discharge coefficient.

Many authors have used a single number, usually ranging from 0.6 to 0.8, as C_d [5-7]; some other researchers have proposed empirical formulas [8- 10]. In both cases, formulas and numbers are derived, and thus are valid, in a very limited range.

In [11], the authors presented a formula for the discharge coefficient of a simple-orifice type feeding system, based on the Reynolds number and on the geometrical parameters of the system, obtained by an extended experimental investigation. Pressure distributions and mass flow rates were measured on pads, whose supply holes had different diameters, under various operating conditions; in particular, the supply pressure and the air film thickness were varied by means of a suitably designed test bench.

A CFD analysis of the pad's feeding system could be an interesting alternative to experimental tests in terms of more cost effective and rapid determination of the discharge coefficient. Some research works were already performed with this method. For example, in [12] a value of critical pressure ratio ranging from 0.35 to 0.4, instead of 0.528, was recommended for calculating the theoretical

mass-flow rate through an annular orifice feeding system, according to CFD simulations confirmed by experimental tests.

The work herein presented deals with the numerical study of the same feeding systems that were experimentally tested in [11]. Comparison between the differently gathered data is, in fact, fundamental in order to choose the most correct physical model for performing simulations.

The influence of the pressure intake needed for carrying out experimental tests on the flow was also evaluated.

2. ANALYSED PAD'S GEOMETRIES

Two aerostatic circular pads made in anodized aluminium, having identical outside dimensions (diameter 40 mm and height 22 mm), were chosen as case on study.

Figure 1a shows a cross sectional view of the pad surface which air is supplied from. Figure 1b highlights the orifice at the centre of the pad and the geometrical parameters characterising the annular flow path: orifice diameter *d*, orifice length *l*, air film thickness *h*. In order to permit pressure measurements along the air film, a flow intake (d_p = 0.2 mm) to be connected to a pressure transducer was provided on one of the pad's surfaces.

As shown in the magnification in Figure 2, all the examined orifices have a fillet or a chamfer between their internal wall and the pad's surface, whose radial dimension *a* is about equal to 5% of the value of the diameter. Table 1 summarises both nominal and measured diameters of the orifices, denoted as *d* and d_{real}, respectively; the measured values, obtained by using an optical fibre microscope (FORT- GLV154 model), are those used in the numerical models. All orifices have a length *l* of 0.3 mm.

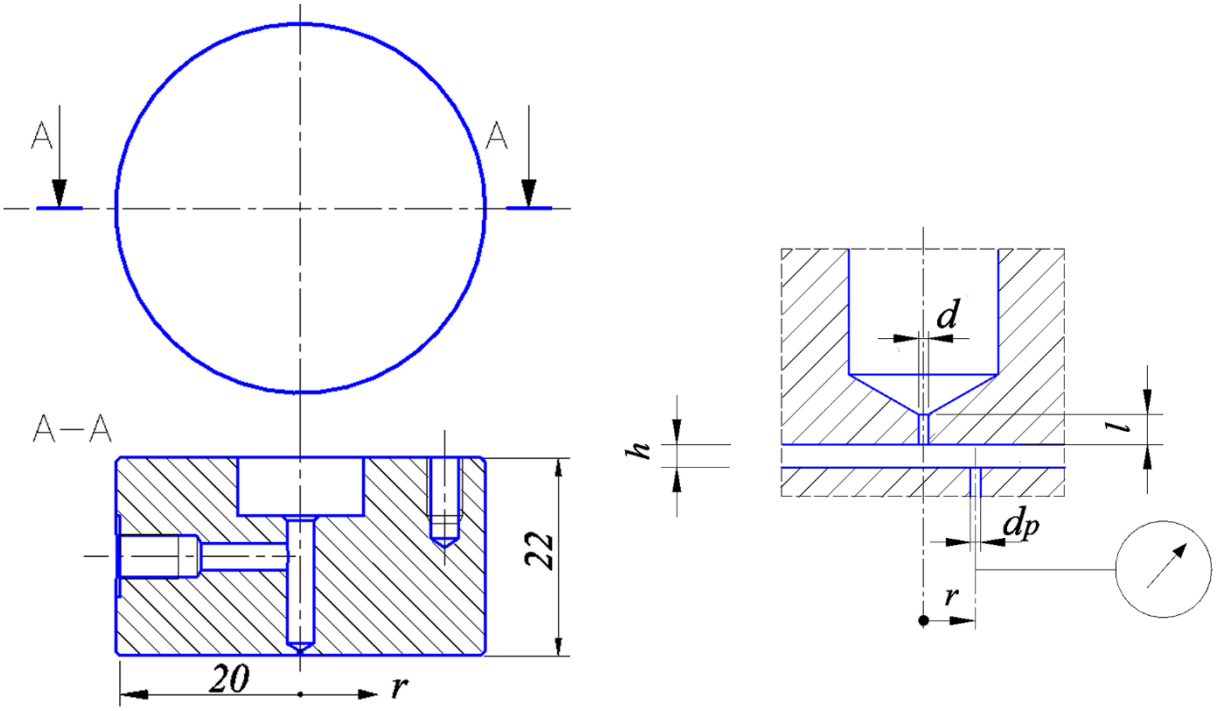

a) b)

Fig. 1 a) Cross-sectional view of the pad under test; **b) Detail of the** orifice, flow intake and related parameters

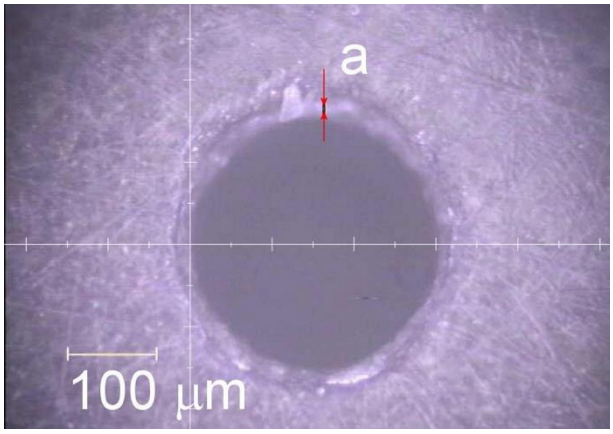

Fig. 2 Magnification of an orifice having a nominal diameter of 0.3 mm

For each pad, air film thicknesses *h* equal to 9, 11, 14 µm were investigated, with a gauge supply pressure p_S equal to 0.5 MPa.

Orifice n°	*d* [mm]	d_{real} [mm]	*a* [μm]
1	*0.20*	*0.23*	*10*
2	*0.30*	*0.31*	*20*

Table 1 Geometry of the orifices under study: nominal and measured dimensions

3. EXPERIMENTAL EQUIPMENT AND PROCEDURE

A test bench was previously constructed which made it possible to measure the static load capability, pressure distribution and air consumption of flat aerostatic pads as a function of the air gap. It consists of a fixed base, over which the stationary pad's member is assembled, and of a movable part, actuated by a screw, carrying the second pad's member provided by the feeding orifice. The air gap height is set by moving the second pad's member vertically and is measured by micrometric transducers placed at three different radial positions. In order to permit pressure measurements along the air gap, the bearing's stationary member, provided by a flow intake (Figure 1b), can be moved radially with respect to the pad under test by means of a micrometric guide. The test bench is equipped by a load cell to measure thrust on the pad and by a float type flowmeter to measure pad's air consumption. More details about the test bench structure can be found in [11].
A rigorous test procedure was defined in order to ensure a good repeatability of results. At first, the pad was supplied by compressed air and loaded with a force high enough to put in contact the movable and the fixed bearing members; in this condition no flow-rate was detected through the pad and the micrometric transducers were set to zero. Then, the load was decreased to set the air gap at the desired height, calculated as the average of the three micrometric transducers' readings; turning air supply off and back on, the repeatability of sensors' measurements were checked and a load correction was applied, if needed. Having set the gap's height, pressure measurements were carried out placing the flow intake at different radial positions along the air gap. During each test, the pad's

supply pressure was kept constant by using a pressure regulator; ambient pressure and temperature of pad's supply air were measured and recorded, respectively, by a barometer and a thermocouple. The same procedure was repeated for each examined value of air film thickness.

4. NUMERICAL SIMULATION OF ANNULAR ORIFICES

The commercial CFD software Ansys Fluent® was employed to numerically determine mass flow-rate through the pad and pressure distribution along the air film. Since the air flow in the pad is axis-symmetrical, a two-dimensional model of the flow field was developed.

Air was assumed to obey to ideal gas law. Upstream of the flow was assumed to have constant total gauge pressure equal to the supply pressure of the pad; downstream of the flow was set at atmospheric pressure. Both laminar and turbulent flow conditions were investigated.

For turbulent flow, results from two different turbulence models, the Spalart-Allmaras and the two-equation k-ε models, were compared. In fact, unfortunately, no single turbulence model is universally accepted as being superior for all classes of problems: for each specific problem an optimum model permitting to avoid numerical diffusion must be found. The Spalart- Allmaras turbulence model, solving only one turbulence transport equation, is a low Reynolds number model designed specifically for flows involving separations and reattachment. The k-ε turbulence model is a semi-empirical model developed for high-Reynolds-number flows. Up to now, it has been used in most practical engineering flow calculations, because of its economy and reasonable accuracy for a wide range of turbulent flows.

For laminar flow, adiabatic (null heat flux through the solid wall boundaries) and isothermal flow conditions were compared. In case of adiabatic conditions, air viscosity μ was calculated as a function of absolute temperature T: $\mu = \mu_0 \cdot (T / T_0)^{2/3}$, where μ_0 and T_0 are respectively air

viscosity and temperature under standard conditions; environmental pressure and temperature values were set equal to those recorded during experimental tests.

A refined mesh was applied close to the orifice, as shown in Figure 3. A fillet having radial dimension a = 10 μm was provided between the orifice's wall and the pad's surface.

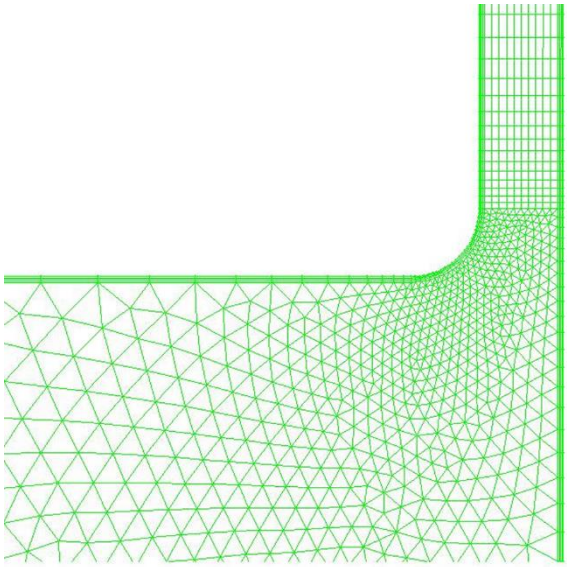

Fig. 3 Grid system used for numerical simulations

4.1 Flow model identification

In order to determine the flow model able to give the best prediction of the pads' behaviour, preliminary simulations were performed on a single pad using a laminar adiabatic model, a laminar isothermal model, a one equation Spalart-Allmaras turbulence model and a two-equation k-ε turbulence model. Results were compared with experimental ones.

The graph in Figure 4a shows pressure distribution along the entire pad, while Figure 4b highlights the air flux behaviour nearby the feeding orifice. Represented data refer to simulations performed on feeding orifice n°1 (Table 1), with its real dimensions, supplied with pressure p_S of 0.5 MPa, having set the air film thickness h to 14 μm.

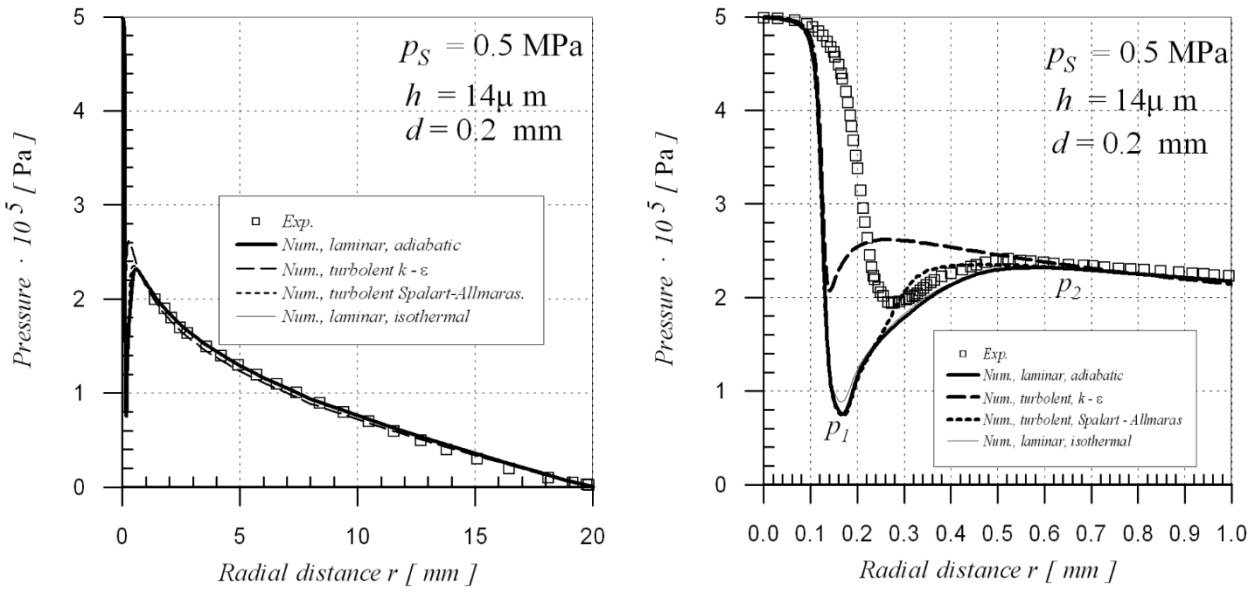

a) b)

Fig. 4 Experimental and numerical pressure distribution. **a)** Along the entire pad; **b)** Close to the feeding orifice

As can be seen, both experimental and numerical data exhibit a pressure drop, more abrupt in the numerical curve, nearby the feeding orifice until a minimum value p_1 is reached. This minimum static pressure value corresponds to a minimum of the air flux area, where a velocity increase occurs. While air flows through the pad, part of the kinetic energy is recovered as pressure energy, so that pressure distribution exhibits a local maximum p_2. From this point, losses are essentially due to viscous forces. It can be seen that the laminar models and the Spalart-Allmaras turbulence model reproduce with good accuracy the pad's behaviour in terms of p_2 value and position. On the contrary, the k-ε turbulence model overestimates the local maximum, whose position is closer to the feeding orifice, and underestimates mass flow-rate through the pad. It can also be noted that the adiabatic and the isothermal laminar models give same results, except a little difference in the value of the local minimum p_1.

Figure 5 shows both static (thin lines) and dynamic (bold lines) numerical pressure distributions, varying the radial distance from the orifice axis to the pad outlet; the dynamic pressure was evaluated in the middle of the air film. It can be noted that the k-ε model calculates a lower flux velocity, corresponding to a wider cross-section of the air flux; this justifies the fact that, using this model, pressure energy is recovered after a shorter radial distance.

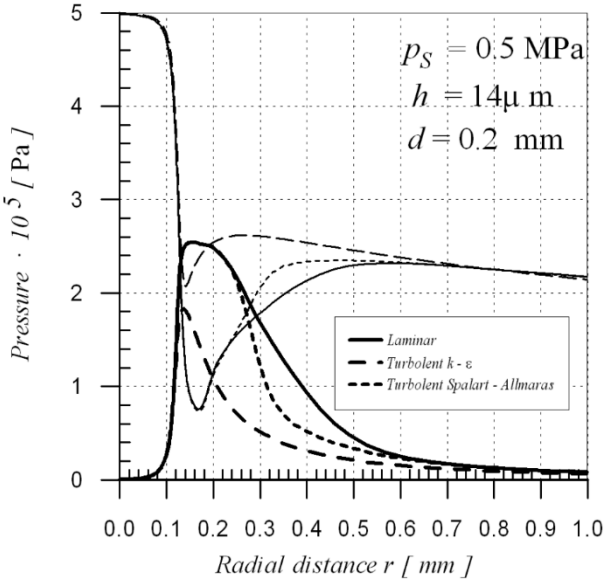

Fig. 5 Static (thin lines) and dynamic (bold lines) numerical pressure distributions

On the basis of this preliminary analysis, the laminar model, which gave good results and was less time consuming, was chosen to perform all following simulations. In particular, since the two laminar models gave almost the same results, with only a small difference close to the feeding orifice, adiabatic conditions were taken into account to perform all the following simulations. In fact, the flow through the feeding orifice can be treated like the flow through a nozzle, without enough time for heat exchange.

5. RESULTS COMPARISON AND DISCUSSION

5.1 Effect of a flow intake on air flux

As discussed in the previous paragraph, numerical results show a good agreement with the experimental ones, in terms of local maximum p_2 and viscous pressure drop.

On the other hand, close to the feeding orifice numerical results exhibit a pressure drop, due to velocity increase, more abrupt than that observed by experimental tests; consequently, dynamic pressure increases as shown in Figure 5. Local minimum p_1 seems to be shifted closer to the orifice axis.

It was considered that experimental pressure distribution along the air film was obtained measuring pressure by means of a pressure transducer connected to a static flow intake manufactured on the movable pad's surface. For a better understanding of the influence of the flow intake, simulations on three-dimensional models of pads equipped with a flow intake were carried out. The flow intake was placed at various radial distances from the axis of the feeding orifice, as it was done during experimental tests. Figure 6 shows an example of simulated geometry.

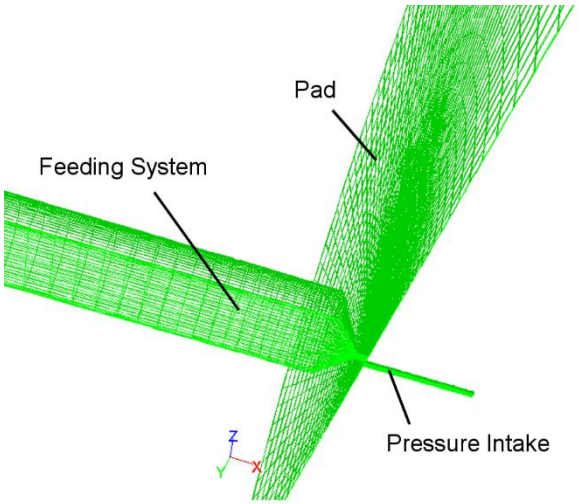

Fig. 6 a Three-dimensional model of a pad, with a static flow intake placed at a radial distance of 0.3 mm from the orifice axis

As an example of the obtained results, Figure 7 compares the velocity flow field close to orifice n°2 (Table 1), supplied at 0.5 MPa and with an air film thickness of 14 μm, without any flow intake and when a flow intake is placed at a radial distance of 0.22 mm from the axis of the orifice. As shown, the presence of the flow intake both modifies the flow field, causing a detachment of the fluid

stream from the pad's surface, and causes an error in pressure measurement; in fact, not only the flow static pressure, but also a part of dynamic pressure is sensed by the measuring instrument.

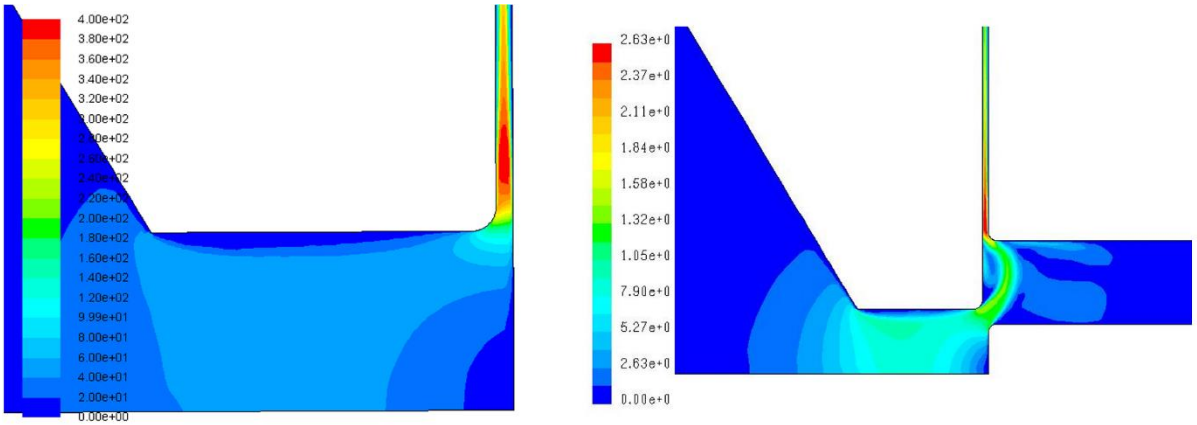

Fig. 7 Velocity flow field of a pad equipped with orifice n°2, supplied at 0.5 MPa, with an air film thickness of 14 μm **a)** Without flow intake; **b)** With a flow intake placed at a radial distance of 0.22 mm from the axis of the orifice

Finally, the graph in Figure 8 compares experimental results, numerical two-dimensional ones and, finally, numerical three-dimensional results obtained placing the static flow intake in four different positions nearby the feeding orifice. According to previous remarks, the use of a flow intake causes a shift of the local minimum in the curve of pressure distribution and an increase in the measured pressure. Nevertheless, the influence of the flow intake was found out to be meaningful only when measuring is made really close to the feeding orifice.

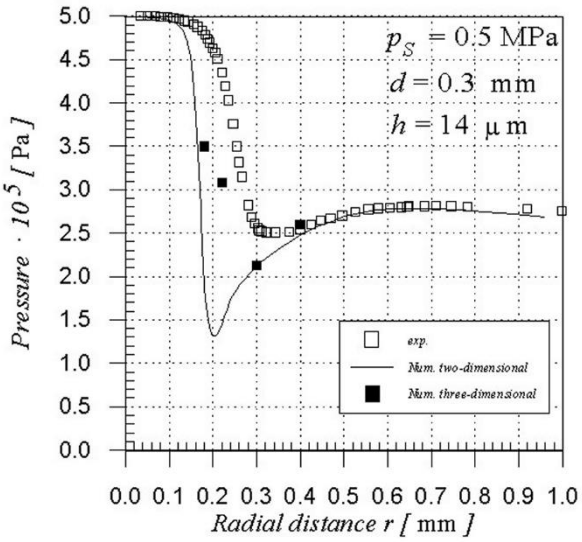

Fig. 8 Pressure distribution along a pad equipped with orifice n° 2: comparison among experimental and numerical 2D and 3D results

Having proved by the 3D model mismatching between numerical and experimental results are due to problems in carrying out experiments close to the feeding orifice without affecting the flow, the 2D axis-symmetric model was used to perform further analysis.

5.2 Influence of smooth or sharp edges in the geometry

The influence of the presence of a chamfer or a fillet, with the same radial dimension, between the wall of the supply orifice and the pad surface, instead of an ideal sharp edge, was also evaluated using the 2D model.

Graph in Figure 9 points out that pressure distribution is not sensitive to the presence of a fillet rather than a chamfer, while a sharp edge causes a higher pressure drop, because of the higher reduction of flow area.

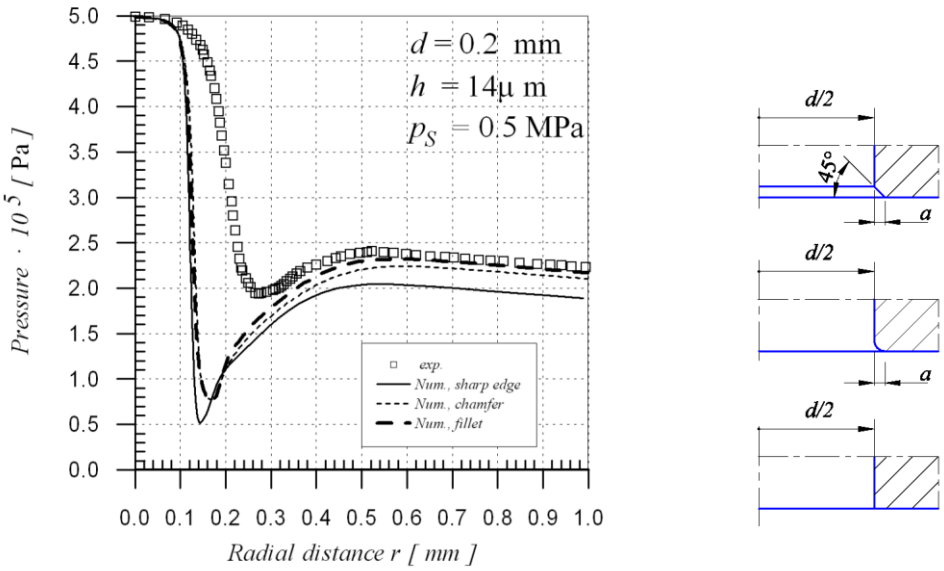

Fig. 9 Comparison of pressure distributions with different shapes of the orifice's external edge

5.3 Influence of the film thickness

Having defined the physical characteristics of the model, further simulations were carried out on axis-symmetrical models of the pads with different diameters d of the supply hole, while varying film thicknesses h.

Table 2 summarises experimental and numerical mass flow rates for all the examined pad's configurations, with a supply pressure of 0.5 MPa. As shown, the higher is the film thickness the lower is the difference between the numerical and the experimental results; setting the film thickness at a precise value during experimental tests, in fact, was not an easy task.

Orifice n°	*h* [μm]	$\dot{m}$ [kg/s] measured	$\dot{m}$ [kg/s] numerical
1	*9*	$1.1 \cdot 10^{-5}$	$0.8 \cdot 10^{-5}$
1	*11*	$1.4 \cdot 10^{-5}$	$1.1 \cdot 10^{-5}$
1	*14*	$1.7 \cdot 10^{-5}$	$1.5 \cdot 10^{-5}$
2	*9*	$1.1 \cdot 10^{-5}$	$0.9 \cdot 10^{-5}$
2	*11*	$1.7 \cdot 10^{-5}$	$1.4 \cdot 10^{-5}$
2	*14*	$2.2 \cdot 10^{-5}$	$2.0 \cdot 10^{-5}$

Table 2 Experimental and numerical mass flow rate through the pad, at a supply pressure of 0.5 MPa

As an example of the obtained results, Figure 10 shows pressure distributions along the pad for feeding orifices n° 1 and 2 (Table 1), while air film thicknesses are set at 9,11,14 μm. In particular, numerical and experimental data are compared nearby the feeding orifices. The matching between numerical and experimental results is in general satisfying, with an exception in case of orifice n°2, with a gap of 9 μm (Figure 10b). This can be ascribed to already mentioned experimental difficulties in setting the air film thickness; nevertheless, the error in identifying the value of p_2 is low (about 5%).

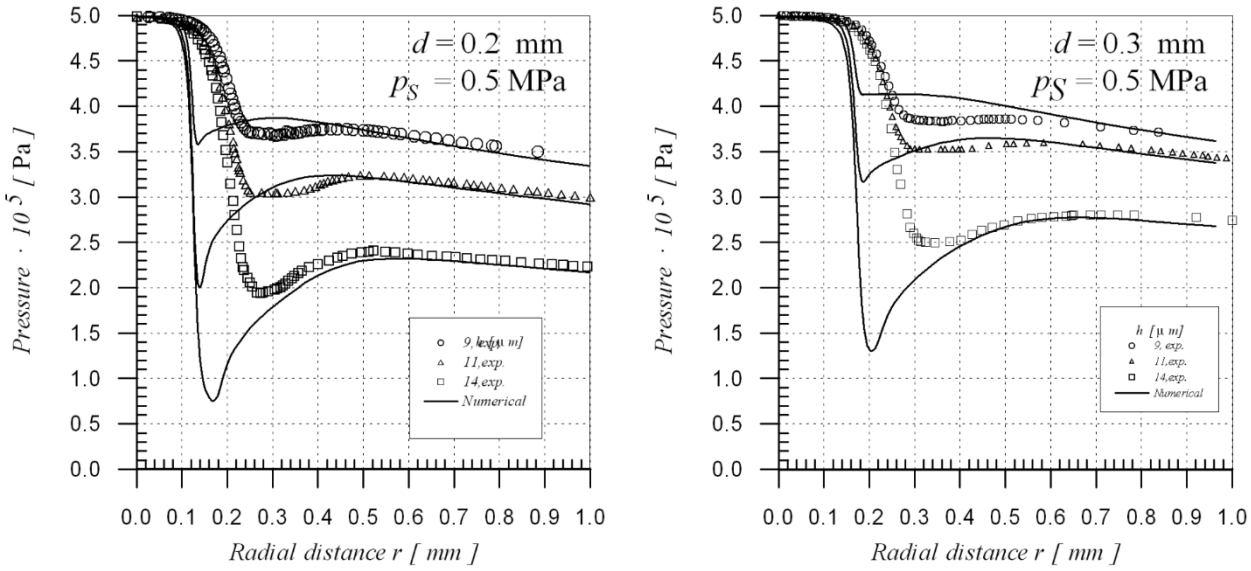

a) b)

Fig. 10 Experimental and numerical pressure distribution varying air film thickness **a)** Close to the feeding orifice n°1**; b)** Close to the feeding orifice n°2

6. DISCHARGE COEFFICIENT

In order to determine the discharge coefficient, the pad under study can be approximated by a simpler pneumatic system consisting of two lumped resistances in series: the orifice's resistance

and the gap's inlet resistance, grouped in a single resistance, causing a first pressure drop; the resistance due to the narrow gap between the pad's surfaces, causing pure viscous losses.

In [11] the theoretical mass flow rate through each resistance was obtained using the isentropic formula for an ideal nozzle:

$$G_t = S \cdot P_u \cdot \sqrt{\frac{k}{k-1} \cdot \left[\left(\frac{P_d}{P_u} \right)^{\frac{2}{k}} - \left(\frac{P_d}{P_u} \right)^{\frac{(k+1)}{k}} \right] \cdot \frac{2}{R \cdot T}} \qquad (2)$$

if $\frac{P_d}{P_u} \geq 0.528$

$$G_t = S \cdot P_u \cdot \sqrt{\left(\frac{2}{k+1} \right)^{\frac{2}{(k-1)}} \cdot \left(\frac{k}{k+1} \right) \cdot \frac{2}{R \cdot T}} \qquad (3)$$

if $\frac{P_d}{P_u} < 0.528$,

where P_u and P_d are the resistances' upstream and downstream absolute pressures, T is the absolute temperature upstream of the nozzle, S is the passage section area, R = 287.1 J/(kg·K) is the air constant, and k = 1.4 is the specific heat ratio of air at constant pressure and volume.

Upstream and downstream pressures were put, respectively, equal to the pad's supply pressure p_S and to the local maximum p_2 of the experimental pressure distribution curve; this way, the airflow behaviour before reaching pressure p_2 did not affect C_d calculation.

For each investigated geometry at varying supply pressures, the discharge coefficient C_d was obtained as the ratio between the experimental flow rate and the theoretical one, according to equation (1). Analyzing and processing the experimental data, the authors proposed in [11] an empirical formula for the discharge coefficient, based on Reynold numbers and on the feeding system's geometry.

Since the numerical results herein presented showed a good matching with the experimental ones in determining the local maximum p_2 of the pressure distribution along the pad, this work confirms the effectiveness of that formula.

7. CONCLUSIONS

Numerical simulations were carried out on aerostatic pads provided by simple orifice-type feeding system and results were compared with experimental ones, previously obtained on the same devices.

Preliminary simulations performed using three different models of the fluid flow showed that the laminar flow model, both considering adiabatic and isothermal conditions, gives the best prediction of the pad's behaviour.

Pressure distribution along the pad is characterized, both in case of experimental tests and numerical simulations, by a first pressure drop nearby the feeding orifice until a minimum value p_1 is reached, followed by a pressure recovery up to pressure p_2. Downstream the local maximum p_2, pressure is reduced only because of viscous forces. Nevertheless, comparing numerical and experimental data, differences can be noted confined in a small zone of the fluid film close to the supply orifice. It was shown that this mismatching can be ascribed to modifications of the flow due to the presence of a pressure intake in the experimental tests. In particular, when measurements are carried out very close to the supply orifice, measured values do not correspond to static pressure, but also part of dynamic pressure is sensed. Conversely, a good agreement between the differently gathered data was found in the zone where pressure drop is purely due to viscous forces.

Since the empirical mathematical formulation for the discharge coefficient C_d previously proposed by the authors was based on pressure p_2, this work confirms the effectiveness of that formula. At the same time, the reliability and the benefit of the numerical approach as a support to experimental tests has been proved.

As aerostatic pads performance is highly dependent on the air film thickness, experimental tests aimed at determining the discharge coefficient C_d required the use of a test bench designed with specific care to ensure high stiffness; furthermore, a rigorous operative procedure had to be applied for ensuring results repeatability. CFD simulations could be a valuable instrument for a quicker analysis of different kind of feeding systems, especially in the phase of selection and optimisation of the most promising geometries.

References

[1] Belforte, G., Colombo, F., Raparelli, T., Trivella, A., Viktorov, V.: Performance of externally pressurized grooved thrust bearings. Tribology Letters 37, 553–562 (2010)

[2] Majumdar, B.C.: Externally pressurized gas bearings: a review. Wear 62, 299-314 (1980)

[3] Belforte, G., Raparelli,T., Viktorov, V.: Theoretical investigation of fluid inertia effects and stability of self-acting gas journal bearings. Journal of Tribology 125, 836-843 (1999)

[4] Al-Bender, F., Van Brussel, H.: Symmetric radial laminar channel flow with particular reference to aerostatic bearings. Journal of Tribology 114(7), 630-636 (1992).

[5] Lund, J.W.: The hydrostatic gas journal bearing with journal rotation and vibration. Journal of Basic Engineering 86, 328-336 (1964)

[6] Bryant, M.R., Velinsky, S.A., Beachley, N.H., Froncza, K.F.T.: A design methodology for obtaining infinite stiffness in an aerostatic thrust bearing. Journal of Mechanisms, Transmissions and Automation in Design 108, 448-456 (1986)

[7] Goodwin, M.J.: Dynamics of rotor-bearing systems. Unwin Hyman, London (1989)

[8] Elrod, H.G., Glanfield, G.H.: Computer procedures for the design of flexibly mounted, externally pressurized, gas lubricated journal bearing. Gas bearing Symposium, University of Southampton, 22.1-22.37 (1971)

[9] Kazimierski, Z., Trojnarski, J.: Investigations of externally pressurized gas bearing with different feeding systems. Journal of Lubrication Technology 102, 59-64 (1980)

[10] Mori, H., Miyamatsu, Y.: Theoretical flow-models for externally pressurized gas bearings. Journal of Lubrication Technology 91, 181-193 (1969)

[11] Belforte, G., Raparelli, T., Viktorov, V., Trivella, A.: Discharge coefficients of orifice-type restrictor for aerostatic bearings. Tribology International 40, 512–521 (2007)

[12] Renn, J-C., Hsiao, C-H.: Experimental and CFD study on the mass flow-rate characteristic of gas through orifice-type restrictor in aerostatic bearings. Tribology International 37 (4), 309-315 (2004)